Journal of Power Sources 195 (2010) 4977–4983

Contents lists available at ScienceDirect

Journal of Power Sources

journal homepage: www.elsevier.com/locate/jpowsour

Mesoporous carbon-encapsulated NiO nanocomposite negative electrode materials for high-rate Li-ion battery

Ming-Yao Cheng [a], Bing-Joe Hwang [a,b,*]

[a] Nano-electrochemistry Laboratory, Department of Chemical Engineering, National Taiwan University of Science and Technology, Taipei 106, Taiwan, ROC
[b] National Synchrotron Radiation Research Center, Hsinchu 300, Taiwan, ROC

ARTICLE INFO

Article history:
Received 8 January 2010
Received in revised form 17 February 2010
Accepted 21 February 2010
Available online 1 March 2010

Keywords:
Mesoporous
Anode
Negative electrode
Lithium ion battery
Nickel oxide
Nanoparticle
High rate

ABSTRACT

In this study, a novel mesoporous carbon-encapsulated NiO nanocomposite is proposed and demonstrated for Li-ion battery negative electrode. The nanostructure of the electrode composes of an ordered mesoporous CMK-3 as a 3D nanostructured current collector with micorporous channels for Li^+ transportation. In addition, exclusive formation of NiO nanoparticles in the confined space of the ordered mesoporous carbon is achieved using the hydrophobic encapsulation route. The half-cell assembled with the synthesized NiO/CMK-3 nanocomposite is able to deliver a high charge capacity of 812 mAh g^{-1} at the first cycle at a C-rate of 1000 mA g^{-1} and retained throughout the test with only 0.236% decay per cycle. Even the C-rate as high as 3200 mA g^{-1}, a charge capacity of 808 mAh g^{-1} contributed by the NiO nanoparticles in CMK-Ni is obtained, which shows excellent rate capability for NiO with utilization close to 100%. The result suggests fast kinetics of conversion reaction for NiO with Li^+. It also indicates the blockage of the pore channels by NiO nanoparticles does not take place in the synthesized NiO/CMK-3.

1. Introduction

The quest for clean energy has made the demand for better energy storage devices a matter of great urgency. Li-ion battery is particular interest because of its high specific energy density [1] and the promising candidate for portable electronics. Recently, promised progress was made in advanced positive electrode materials with high-rate charging/discharging capability and excellent capacity retention, for example, $LiFePO_4$/C [2–5], doped $LiFePO_4$ [6], $LiNi_{0.5}Mn_{0.5}O_2$ [7,8] and spinel [9,10]. When it comes to negative electrodes, lithium titanites are able to exhibit high rate performance [11,12]. Material of high-rate capability and high capacity is still exploited. Most of the ongoing researches for negative electrode materials are focused on how to compensate for the existing drawbacks. For instance, some metal and semiconductor materials (Si, Al, Sn, etc.) form alloys with lithium at a potential that is slightly higher than that of Li^+/Li. These materials possess very high theoretical specific capacities compared with commercial graphite (4,200 mAh g^{-1} for $Li_{4.4}Si$ and 372 mAh g^{-1} for LiC_6). Unfortunately, these Li-alloys are subject to very large volume expansions with respect to their parent materials (e.g. a 200% expansion from Al to Li–Al alloy). After several alloying/de-alloying cycles cracking and crumbling of the active materials take place [1]. The fracture of these active materials leads to loss of electronic contact in the electrode matrix and subsequently reduces the capacity of the battery. In order to compensate this shortcoming, several studies focused on employing the concept in regard to active/inactive composite concept to alleviate the volumetric changes during cycling, such as Sn–Fe–C [13], Si–C [14], Cu_6Sn_5 and InSb [15]. These materials display significant improvements to capacity retention, but less benefit is shown for their rate capability.

Continuous efforts on novel electrode materials with the characteristic of intrinsic high-rate capability are important. On the other hand, it can be achieved by successful design of nanostructured electrodes as well. The reasons include: (i) providing a shorter path length for Li^+ transport from/to the bulk electrolyte phase, (ii) providing a shorter path length for electron transfer from/to the current collector, and (iii) a better stability of the nanostructured electrode matrix during charging/discharging [16]. It is realized by replacing the planar foil with a 3D current collector coated with thin nanostructured active materials to increase the efficiency of the current collection, i.e. shorten the path length of the electron transfer. Taberna et al. fabricated Cu nanorods using electro-deposition with AAO (anodized aluminum oxide) membranes as the templates, which is followed by electro-depositing Fe_3O_4 films onto the Cu nanorods as the negative electrodes [17]. Electrodes made of commercially available metal foams with active materials electro-

* Corresponding author at: Sect. 4, Keelung Rd., Taipei, 106, Taiwan, ROC. Tel.: +886 2 27376624; fax: +886 2 27376644.
E-mail address: bjh@mail.ntust.edu.tw (B.-J. Hwang).

0378-7753/$ – see front matter © 2010 Elsevier B.V. All rights reserved.
doi:10.1016/j.jpowsour.2010.02.059

deposited on are also viable for this concept [18,19]. The thin nanostructured active materials are able to show excellent rate capabilities and capacity retention during charging/discharging.

For the electrode constituted of powdered active materials, conductive additives and binders, higher capacity can be delivered than that of the thin film electrode. In some cases, it is matter of importance for high power applications, for example, power sources for EV/HEV. Therefore, control of the micro-/nanostructure of the electrode is certainly determinative to the electrochemical performance. In fact, carbon is one of the best materials for acting as the current collector. Its fair conductivity, good chemical stability, and light-weight nature make carbon a good choice for most of the electrodes of the energy storage devices, e.g. catalyst supports for fuel cell electrodes and materials for improving the electronic conductivity of the electrodes for capacitors and batteries [20]. However, continuous electron pathway in the electrode microstructure, even nanostructure, cannot be easily formed by only addition of carbon since electrons pass low-electronic conductivity active materials cannot be avoided in the electrode matrix. Therefore the use of nanostructured carbon matrix can work as a 3D nanostructured current collector extended from a planar metal foil with continuous nanochannels serving as the Li^+ ions pathway. In the present paper we demonstrate this concept with ordered mesoporous CMK-3 as the nanostructured current collector and the nano-sized NiO as the active material inside the nanochannels of CMK-3. The NiO/CMK-3 nanocomposite is prepared using the developed hydrophobic encapsulation route in our previous study [21]. The blockage of the nanochannels is not observed in the mesoporous hosts, which is crucial for species to access the nanoparticles in the ordered mesoporous hosts [22,23]. It is found that the poor electrochemical performance of NiO in the literature [24,25] is able to turn to electrochemically active in our work. The results strongly support the proposed concept, which is of potential for other electrochemical applications.

2. Experiment

2.1. Synthesis

All chemicals were purchased from Acros (except poly(ethylene glycol)-block-poly(propylene glycol)-block-poly(ethylene glycol), P-123 from Aldrich) and were used as-received. The process for the material synthesis is illustrated in Fig. 1. Mesoporous CMK-3 was prepared by the procedure reported by Jun et al. [26]. In this procedure, mesoporous SBA-15 was first synthesized and calcined at 823 K for 3 h to remove organic moieties (Step a, Fig. 1). Then the calcined SBA-15 was impregnated with sucrose solution containing 1.25 g of sucrose, 0.14 g of H_2SO_4, and 5 g of H_2O. The mixture was baked in the oven at 373 K for 6 h and then at 433 K for another 6 h. The impregnation and baking processes were repeated again, but changing the composition of the solution to 0.8 g of sucrose, 0.08 g of H_2SO_4 and 5 g of H_2O. Afterwards, the dried mixture containing partial polymerized carbon precursor and SBA-15 was placed in the furnace and carbonized at 1173 K for 3 h in nitrogen (Step b, Fig. 1). The carbonized powders were washed with 2 M NaOH solution (50 vol% ethanol–50 vol% water) twice to remove silica (Step c, Fig. 1). The composition of the as-prepared CMK-3 was confirmed by the energy dispersive X-ray spectroscopy (EDS), and only traces of silica were left (0.2 wt%, data not shown).

The hydrophilic encapsulation route developed in our previous study [21] was employed for the synthesis of NiO nanoparticles in the mesoporous CMK-3 matrix. Simply speaking, 1 g of the acid-treated CMK-3 (in H_2SO_4 at 373 K for 3 h) was fully impregnated with the concentrated nickel precursor solution (0.035 mol (99%) nickel nitrate hexahydrate and 0.0175 mol citric acid in 5 g of the de-ionized water) with stirring (Step d, Fig. 1). The mixture was then poured into a centrifuge filter followed by addition of n-octane. The centrifugal process was performed at 7000 rcf and 298 K for several cycles. The process continued until very little or no precursor solution was observed in the reservoir of the centrifuge filter (Step e, Fig. 1). Then the powders were collected, dried, and heated at 673 K for 1 h at a heating rate of 2 K per minute in nitrogen. The product was named CMK-Ni (Step f, Fig. 1).

2.2. Characterization

To determine the content of NiO, thermal gravimetric analysis (TGA) of the CMK-Ni was performed with a thermal gravimetric analyzer (Perkin-Elmer Diamond series) with a ramping rate of 10 K per minute to 1173 K in flowing air. The ordering of the mesostructure was analyzed by an Osmic small angle X-ray scattering system (model PSAXS-USH-WAXS-002, USA) with a Cu Kα radiation source and operated at 45 kV and 0.67 mA. The crystalline structure of the sample was characterized by an X-ray diffractometer (Rigaku D/Max-RC, Japan) with a Cu Kα as the radiation source and operated at 40 kV and 100 mA. Transmission electron microscopy (TEM) analysis was performed with JEOL JEM-2010 operated at an accelerating voltage of 200 kV. For preparation of the TEM sample, 0.01 g of the powder was added to 20 mL ethanol with ultrasonic treatment for 30 min. Later, 0.05 mL of the solution was dropped onto a lacey carbon-coated Cu grid and dried at 353 K. Nitrogen adsorption–desorption analysis was performed with a Quantachrome AUTOSORB-1 at 77 K in a liquid nitrogen bath. The surface area of the sample was calculated by the Brunauer–Emmett–Teller (BET) method. Pore size distribution of the product was obtained according to the Barrett–Joyner–Halenda (BJH) method.

For evaluating the electrochemical performance of the materials, a mixture of 85 wt% CMK-Ni and 15 wt% polyvinylidene fluoride (PVDF) in N-methyl-2-pyrrolidone (NMP) was taken as the slurry for casting. The slurry was cast on the Cu foil followed by drying at 353 K overnight. The cast Cu foil was punched into a 1.3 cm^2 circle as the electrode of about 50 μm in thickness. The active material on the electrode is around 1 mg cm^{-2}. The packing density is around 11.0% for the electrode with CMK-3 or CMK-Ni and 28.5% for the electrode with CA-NiO (97%, 25–30 nm in grain size). The difference in packing density between CMK-3 (or CMK-Ni) and CA-NiO is owing to the difference of the corresponding specific density for CMK-3 (or CMK-Ni). The coin cell was assembled in an argon-filled glove box with the prepared electrode as the cathode and the Li metal as the anode. The two electrodes were separated by a polypropylene separator saturated with 1 M $LiPF_6$ electrolyte solution (Tomiyama, EC:DEC = 1:1 in weight ratio). The charging/discharging behavior of all the cells was galvanostatically cycled between 3 and 0.01 V. Capacity retention tests of the assembled cells were carried out for the required rates. Rate capability tests of the cells were performed by changing the rate from 100 to 3200 mA g^{-1} (10^{-4} to 3.2×10^{-3} A cm^{-2}) for each 5 cycles. For comparison, the electrodes prepared with CMK-3 and CA-NiO (commercial available NiO) received the same procedure as the CMK-Ni electrode. The specific capacity is based on the weight of the active materials in the electrode (e.g. for CMK-3 and CMK-Ni electrodes, the specific charge/discharge current density is based on the weight of CMK-3 and CMK-Ni (binder is excluded). For CA-NiO electrode, only NiO is accounted for the calculation (binder and carbon black is excluded).

3. Results and discussion

The content of NiO in CMK-Ni is firstly confirmed by TGA. It is about 36.6 wt% of NiO in CMK-Ni (92.3 wt% at 423 K and 33.7 wt% at

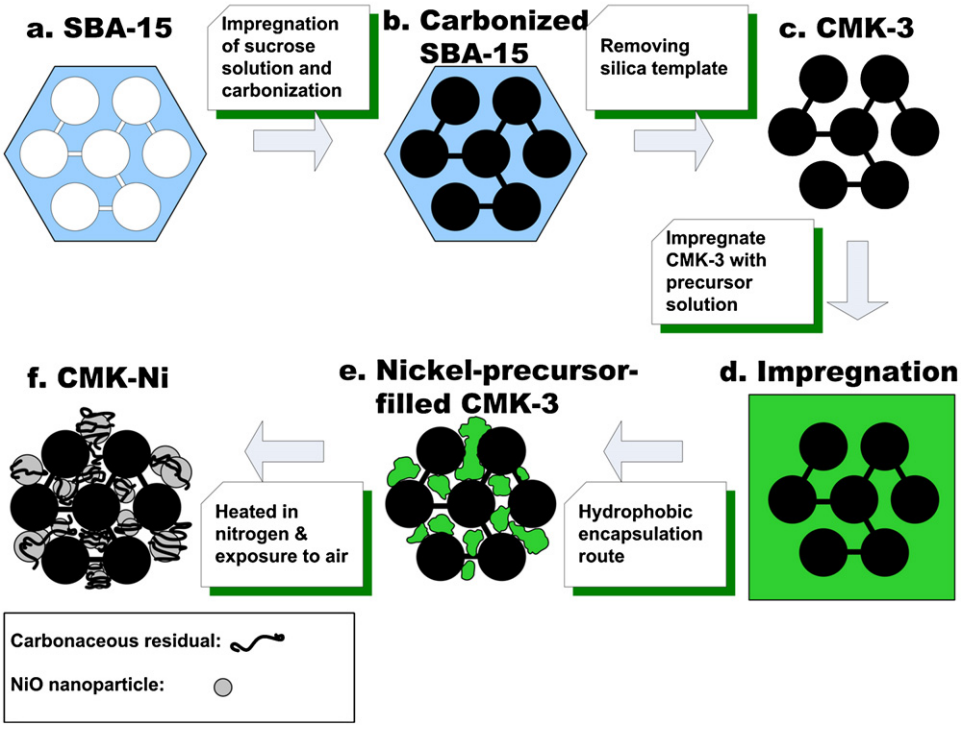

Fig. 1. Schematic illustration for the synthesis of CMK-Ni.

1173 K, data not shown). It should be noticed that the carbonaceous residuals originated from pyrolysis of citric acid contribute parts of the weight loss and are difficult to differentiate from that of CMK-3. Further, the formed carbonaceous residuals may occupy part of the confined space of the CMK-3 as well.

Low-angle XRD patterns for CMK-3 and CMK-Ni are shown in Fig. 2(a). Three intense peaks corresponding to the periodic two-dimensional hexagonal (*P6mm*) mesostructure with a lattice parameter of 9.55 nm (d_{100} = 8.27 nm at 2θ = 1.067 degree) are observed. For CMK-Ni, the absence of peaks in the low-angle range indicates that there is no periodic mesostructure after incorporation of NiO. This lack of mesostructure periodicity for CMK-Ni is possibly due to the relatively low contrast of carbon backbone to pore channels, which are largely filled by the formed materials. A wide-angle XRD pattern for CMK-Ni is shown in Fig. 2(b). All the peaks correspond to the face-centered cubic crystalline structure of NiO (JCPDS-ICDD no. 78-0429), except one broad peak centered at 2θ around 25.2 degrees owing to the amorphous carbon rods of CMK-3. The formation of NiO indicates the success of spontaneous oxidation of the fine Ni nanoparticles after exposure to air since the organic part (citric acid) of the precursor should decompose first to form carbonaceous residuals, and the nickel species confined in the nanochannels could be reduced to form fine Ni nanoparticles in the presence of the carbonaceous residuals and CMK-3 during heating in nitrogen. It is difficult to form/control transition metal oxides/carbon nanocomposites using other methods because heating is usually needed in oxygen-containing atmosphere for the formation of transition metal oxides. However, in most of the cases, burning of the carbon cannot be avoided. In our case, the difficulties in the synthesis of transition metal oxides/carbon nanocomposites could be overcome with the developed route, in which the nickel precursor solution is able to fill the nanochannels completely without the existence of the bulk phase outside the CMK-3. Hence, the size of the nickel particles, which are only formed in the nanochannels of the CMK-3, is limited. It is evident that the average grain size of the formed Ni particles is only a few nanometers and is able to be oxidized spontaneously after exposure to air. From the Scherrer equation with the full width at half maximum (FWHM) of the (2 0 0) peak, the average grain size of NiO is about 1.94 nm, which confirms that the initially formed nickel nanoparticles are small enough to form NiO nanoparticles spontaneously in air.

Fig. 3(a) shows the low magnification TEM image of the as-prepared CMK-3. The uniform nanochannels are clearly observed, indicating the successful synthesis of the CMK-3 (inset of Fig. 3(a)). For CMK-Ni, the low magnification TEM image shows tremendous nickel oxide nanoparticles embedded in the CMK-3 (Fig. 3(b)). The image shown in Fig. 3(b) is taken in off-axis direction for the ordered mesoporous materials, which the intensity contributed from the support (ordered mesoporous materials) can be averaged. Therefore, the small dots clearly observed in Fig. 3(b) are contributed from the NiO nanoparticles. In addition, no larger particles are observed outside the nanostructure of the CMK-3, which means an effective encapsulation of the formed NiO nanoparticles in the mesoporous CMK-3. Fig. 3(c) shows how the nanoparticles line up along the pore channels of CMK-3. The image is taken with the electron beam perpendicular to the pore channels. From Fig. 3(b) and (c), it seems that the size of the NiO nanoparticles in CMK-Ni is quite small, but not uniformly distributed. Therefore a high magnification image was taken to resolve the doubt (Fig. 3(d)). Actually, the particles can be classified into two groups, one group with a size of 2 nm and the other with a size of 5 nm, as shown in Fig. 3(d). The diversity of the NiO particle sizes in CMK-Ni is possibly the result from the two different environments available for confining the Ni precursor solution in CMK-3 during the preparation. The group of the NiO nanoparticles with the 2 nm size is possible pinned in the inner nanochannels of the CMK-3 whereas the other group with the 5 nm size should be located at the exterior nanochannels, which may be partially open to atmosphere.

The physical properties of CMK-3 and CMK-Ni are characterized by nitrogen adsorption/desorption isotherms as shown in Fig. 4(a). The absorption/desorption hysteresis between the P/P_0 range of 0.4 and 0.75 for CMK-3 is typical for mesoporous materials. In con-

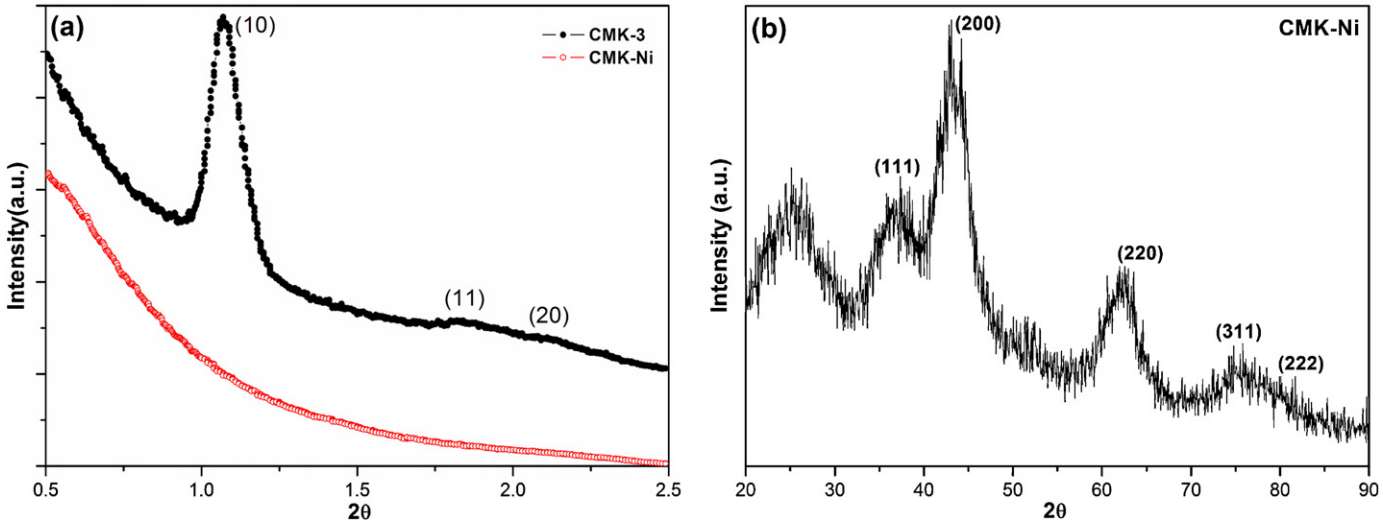

Fig. 2. XRD patterns for CMK-3 and CMK-Ni. (a) Low-angle XRD pattern for CMK-3 and CMK-Ni. (b) Wide-angle XRD pattern for CMK-Ni (Indexing is based on JCPDS-ICDD no. 78-0429).

trast, CMK-Ni shows no adsorption/desorption hysteresis in this P/P_0 range, indicating that almost all the nanochannels of CMK-3 are fully filled with the NiO nanoparticles accompanied with carbonaceous residuals. This observation supports the absence of the periodity for CMK-Ni by low-angle XRD analysis because it seems that the formed NiO nanoparticles and carbonaceous residuals occupy a large proportion of the pore volume of CMK-3. Further, the BET surface area decreases from 1754 $m^2\,g^{-1}$ for CMK-3 to 625 $m^2\,g^{-1}$ for CMK-Ni (see Table 1), which is consistent with the proposed high occupation degree of nanochannels in CMK-Ni. The pore size distributions of CMK-Ni and CMK-3 (Fig. 4(b)) also reveal that most of the nanochannels in CMK-Ni are occupied. The mesopore volume decreases from 0.7126 $cm^3\,g^{-1}$ for CMK-3 to 0.0737 $cm^3\,g^{-1}$ for CMK-Ni, as shown in Table 1. The micropore volume, decreasing from 0.7474 $cm^3\,g^{-1}$ for CMK-3 to 0.2938 $cm^3\,g^{-1}$ for CMK-Ni, indicates that fair amounts of micropores in the CMK-Ni are still preserved. This is assumed to be the fact that some micropores in the carbon rods are not accessible to the nickel precursor solution during preparation. On the other hand, it is also possible that parts of the micropores are created by the occupied nickel oxide/carbon residual composite in the mesopore channels.

The rate capability of the CMK-Ni electrode was firstly investigated to understand its performance as the negative electrode of the Li-ion battery. Owing to the difficulty of determining the theoretical capacity of CMK-3, we galvanostatically cycled the assembled battery with the current density based on the weight of the active materials. As shown in Fig. 5(a), the cell assembled by the CMK-Ni electrode delivers a high charge capacity of 1152 mAh g^{-1} at the low C-rate of 100 mA g^{-1}. The high capacity of CMK-Ni electrode is comparable to that of the pure CMK-3 electrode (1217 mAh g^{-1}). Even though a CMK-3 electrode can deliver a high charge capacity, as investigated in literature [27], the irreversible capacity at the first cycle is more than twice the value to that of the CMK-Ni electrode (1392 mAh g^{-1} for pure CMK-3 to 604 mAh g^{-1} for CMK-Ni). The high first-cycled irreversible capacity of CMK-3 limits its practical use as the negative electrode of the Li-ion batteries since large portion of Li ions from the cathode side will be consumed, which would lead to a low specific capacity and low power density of the full cell. Surprisingly the high first-cycled irreversibility is greatly reduced for CMK-Ni, which the reversible capacity is comparable to that of CMK-3. For CA-NiO, the first-cycled charge capacity and irreversible capacity is 873 and 411 mAh g^{-1} (100 mA g^{-1} is about 0.14C for NiO, 1C: full use of capacity in 1 h), respectively, which is typical in the literature [24]. The specific capacity for CA-NiO is higher than its theoretical value, which may be resulted from the involvement of partly reversible formation/dissolution of the polymeric layers on NiO particles [28,29]. The polymeric layer involves a faradic process of organic electrolyte taking place on active materials. Comparing CMK-Ni with the CA-NiO, the ratio of first-cycled charge capacity to the corresponding discharge capacity is almost the same (68.0% for CA-NiO and 65.6% for CMK-Ni). Nevertheless, the first-cycled irreversible capacity for CMK-Ni should be contributed from (i) the surface hydrogen or oxygen site and corrosion-like reaction of Li_xC_6 that are common for high specific energy capacity carbons (X = 1.2–3.0) [27], and (ii) the formation of polymeric layers on the NiO surface. Hence, the only possibility for the apparent reduction in irreversible capacity for CMK-Ni should be the formation of the NiO/carbonaceous residuals in the nanochannels of the parent CMK-3 host, in which the access of the electrolyte solution to the CMK-3 surface is limited. This subsequently reduces the formation of polymeric layers on the CMK-3 surface since the formed polymeric layers on the carbon surface are reported to be irreversible [28] and not involved in the electrochemical activity of the following cycles. It is evident by the reduction of 64.36% in the specific BET

Table 1
Physical properties of CMK-3 and CMK-Ni.

	BET ($m^2\,g^{-1}$)[a]	Average pore size (nm)[b]	Micropore volume ($cm^3\,g^{-1}$)[c]	Mesopore volume ($cm^3\,g^{-1}$)[d]	Lattice parameter (nm)[e]
CMK-3	1754	3.6	0.7474	0.7126	9.55 nm
CMK-3-Ni	625	2.6	0.2938	0.0737	n.a.

[a] Calculated with the BET method.
[b] Accumulated pore volume with P/P_0 lower than 0.949.
[c] Obtained from N_2 absorption isotherm with the BJH method at P/P_0 smaller than 0.19935.
[d] Obtained from N_2 absorption isotherm with the BJH method at P/P_0 between 0.19935 and 0.95107.
[e] Calculated from d_{100} spacing with $a = d_{100}(2 \times 3^{-0.5})$.

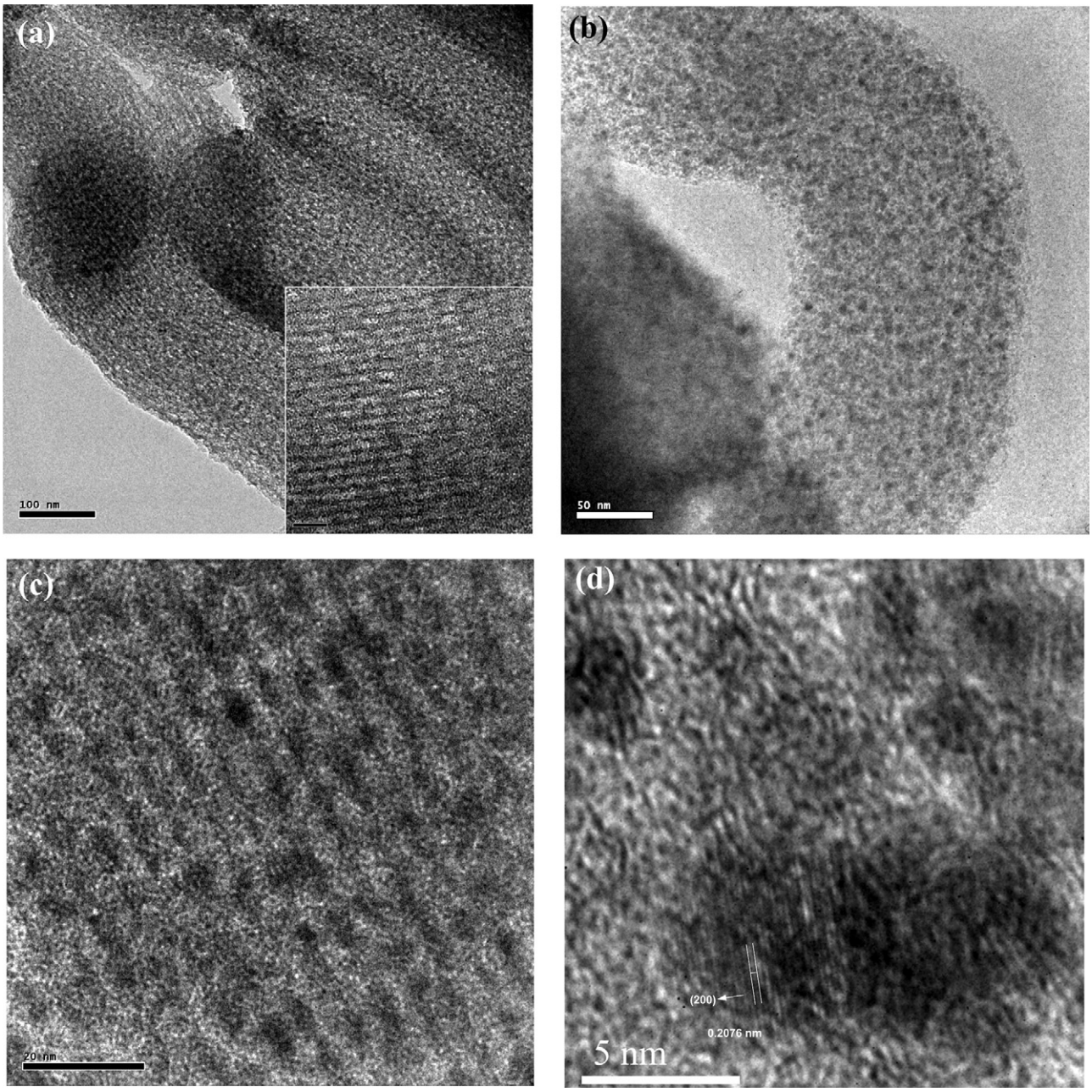

Fig. 3. TEM images of (a) as-prepared CMK-3 and (b, c, and d) CMK-Ni. (a) Low magnification image, scale bar: 100 nm. Inset: higher magnification image of CMK-3, scale bar: 20 nm. (b) Low magnification image, scale bar: 50 nm. (c) Image with electron beam perpendicular to the pore channels of CMK-Ni, scale bar: 20 nm. (d) High resolution image of NiO in CMK-Ni with lattice image of (2 0 0) plane, scale bar: 5 nm (images obtained by JEOL JEM-2010 transmission electron microscope).

surface area from CMK-3 (1754 $m^2\,g^{-1}$) to CMK-Ni (625 $m^2\,g^{-1}$). It also implies that even the loading of NiO is not high, however, the first-cycled irreversible capacity contributed from CMK-3 can be greatly reduced. It is another benefit for employing CMK-Ni with the presenting nanostructure.

At the high C-rate of 3200 mA g^{-1}, CMK-Ni still shows excellent cycling behaviors with a stable charge capacity of 413 mAh g^{-1}, which is about 2.23 times to CMK-3 and 2.47 times to CA-NiO with a columbic efficiency of 99.52%. If we only consider the contribution of NiO in CMK-Ni by simply subtracting the contribution of CMK-3 at the C-rate of 3200 mA g^{-1} (weight percent of CMK-3 in CMK-Ni multiples its specific capacity), a charge capacity of 808 mAh g^{-1} contributed by the NiO nanoparticles in CMK-Ni is then obtained. This result implies excellent rate capability for NiO nanoparticles in CMK-Ni with almost 100% utilization, even cycling at high C-rate. In this case, the contribution of CMK-3 to the capacity of the CMK-Ni electrode is much less than that of NiO. This indicates that CMK-3 in the CMK-Ni electrode acts as an excellent 3D nanostructured current collector for electron transfer during the redox reaction of NiO nanoparticles. In addition, the excellent electrochemical properties imply the micropores existing in CMK-Ni should act as the pathway for Li^+ ions transportation. The shorter path lengths for electrons transfer and Li^+ transport can be realized with the CMK-Ni nanocomposites.

Fig. 5(b) shows the capacity retention test of the cells cycled at 1000 mA g^{-1} for 50 cycles. The cell with a CA-NiO electrode exhibits a stable capacity around 410–430 mAh g^{-1} up to the 15th cycle. After the 15th cycle, the capacity drops dramatically and only 85 mAh g^{-1} is obtained at 50th cycle. The poor capacity retention of NiO is similar to previous reports, even cycling

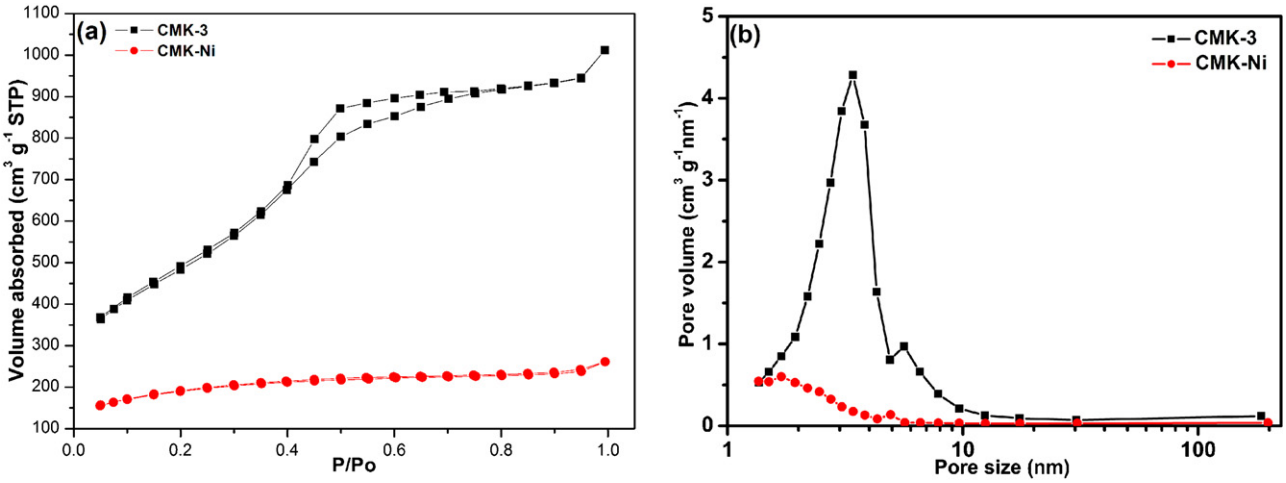

Fig. 4. (a) Nitrogen adsorption/desorption isotherms and (b) Pore size distribution of CMK-3 and CMK-Ni.

at a low C-rate [24,25]. For the CMK-Ni electrode, a high capacity is retained throughout the test with only 0.236% decay per cycle (charge capacity of 812 mAh g^{-1} at first cycle and 716 mAh g^{-1} at the 50th cycle). The contribution of NiO in the CMK-Ni electrode is again calculated and is around 1426 mAh g^{-1}, which is twice the theoretical value of NiO (717 mAh g^{-1}). This large bonus capacity is likely due to the reversible formation/dissolution of the polymeric layer on NiO nanoparticles [28,29] in CMK-Ni

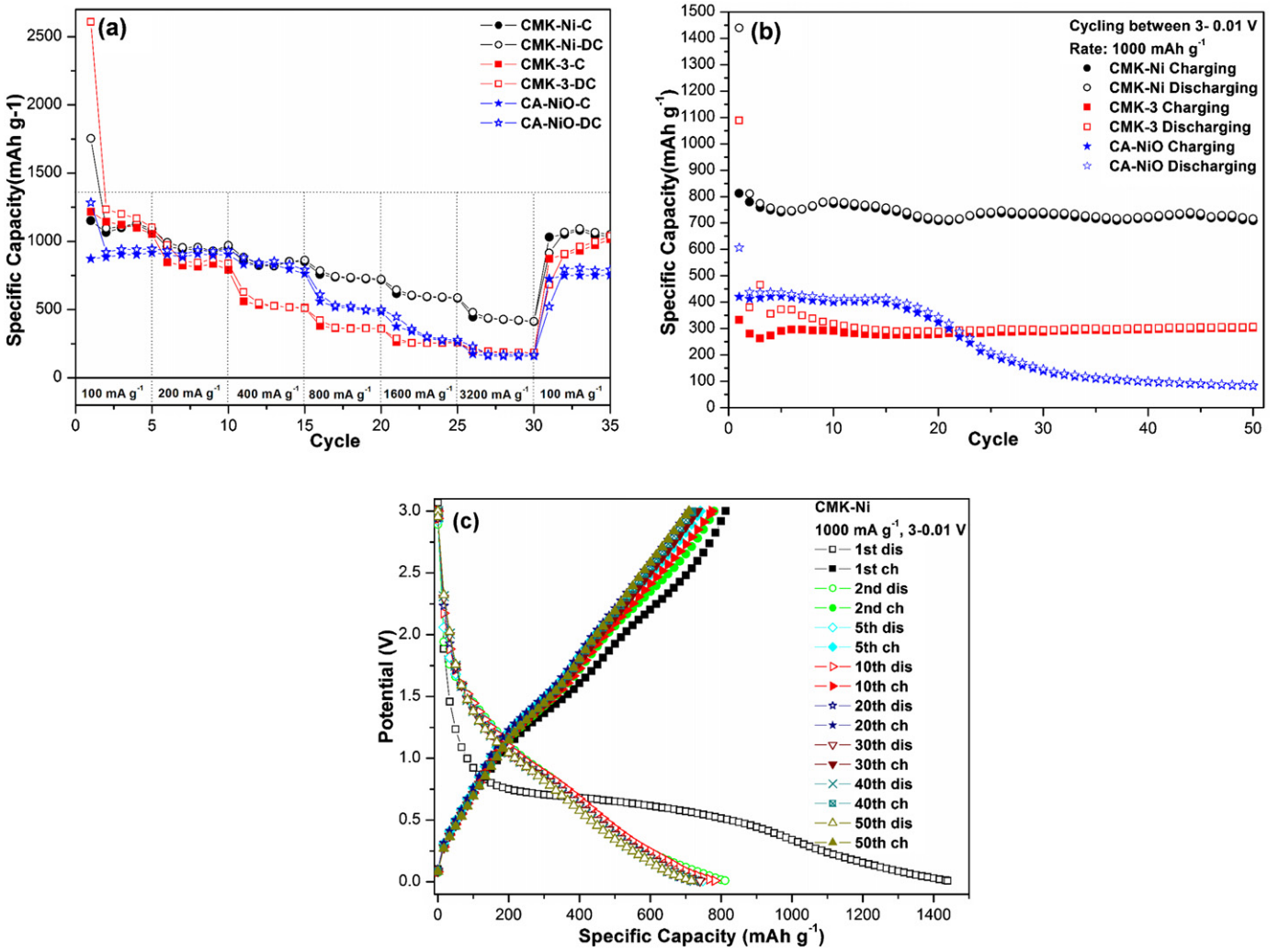

Fig. 5. Electrochemical performances of CMK-Ni, CMK and CA-NiO. (a) Rate capability tests of the cells assembled by CMK-Ni (circle), CMK (square) and CA-NiO (asterisk) electrodes; hollow: discharge state, filled: charge state. (b) Capacity retention test of the cells assembled by CMK-Ni (circle), CMK (square) and CA-NiO (asterisk) electrodes cycling at a rate of 1000 mAh g^{-1}; hollow: discharge state, filled: charge state. (c) Potential-capacity relationship of the cells assembled by CMK-Ni electrode with a cycling rate of 1000 mAh g^{-1}.

since small NiO nanoparticles provide a large surface area for polymeric layer formation. Furthermore, the electronic pathway provided by the 3D nanostructured current collector may be the reason for the high reversibility of the polymeric layer on the NiO nanoparticles. It is suggested that the formation/dissolution of the polymeric layer on the NiO surface may be hindered when the cell is cycled at a higher C-rate. This assumption is supported by the high specific capacity (1426 mAh g^{-1}) contributed by NiO for CMK-Ni cycled at the rate of 1000 mA g^{-1} while only 808 mAh g^{-1} is obtained at the rate of 3200 mA g^{-1}. This is probably related to the time constant of the formation/dissolution process for the polymeric layer on the NiO surface. Further investigation is conducted for resolving this point and will be reported elsewhere.

The galvanostatic charge/discharge behavior for the cell with a CMK-Ni electrode cycled between 3 and 0.01 V at a rate of 1000 mA g^{-1} is shown in Fig. 5(c). The stable charge capacity is obtained after the first cycle. The large hysteresis loop between the charging and discharging process of CMK-3 [27] is greatly reduced with the incorporation of the NiO nanoparticles within the nanochannels. The excellent cycling behavior of CMK-Ni is thus observed.

4. Conclusion

In this work, we have demonstrated the mesoporous CMK-3-encapsulated NiO nanoparticles can be achieved by spontaneous oxidation of Ni nanoparticles using the developed hydrophobic encapsulation route. NiO nanoparticles are able to embed in the nanochannels without full blockage. In the synthesized CMK-Ni, CMK-3 can play the role as the 3D nanostructured current collector and the micropores in the nanochannels can be the path for Li^+ transportation. The novel nanostructure is able to provide 100% utilization for the NiO active materials at high cycling rate, which indicates a promised application as the negative electrodes for high-rate Li^+ batteries. When comparing with the poor behavior of NiO reported in the literature, the excellent capacity retention for CMK-Ni is observed. The present concept is a basic approach to create continuous electronic and ionic pathways impregnating into the active materials. This novel nanostructure of metal oxides/mesoporous carbon nanocomposites addressed here can also be applied to other systems for various interesting electrochemical reactions.

Acknowledgements

The authors thank the financial supports from the National Science Council of Taiwan (under contract numbers NSC 97-2120-M-011-001-, and NSC 98-ET-E-011-003-ET) and technical supports from National Synchrotron Radiation Research Center (NSRRC), National Taiwan University of Science and Technology (NTUST).

References

[1] J.-M. Tarascon, M. Armand, Nature 414 (2001) 359.
[2] Z. Chen, J.R. Dahn, J. Electrochem. Soc. 149 (2002) A1184.
[3] C.R. Sides, F. Croce, V.Y. Young, C.R. Martin, B. Scrosati, Electrochem. Solid-State Lett. 8 (2005) A484.
[4] K.F. Hsu, S.Y. Tsay, B.J. Hwang, J. Mater. Chem. 14 (2004) 2690.
[5] B.-J. Hwang, K.-F. Hsu, S.-K. Hu, M.-Y. Cheng, T.-C. Chou, S.-Y. Tsay, R. Santhanam, J. Power Sources 194 (2009) 515.
[6] S.-Y. Chung, J.T. Bloking, Y.-M. Chiang, Nat. Mater. 1 (2002) 123.
[7] K. Kang, Y.S. Meng, J. Bréger, C.P. Grey, G. Ceder, Science 311 (2006) 977.
[8] B.-J. Hwang, T.-H. Yu, M.-Y. Cheng, R. Santhanam, J. Mater. Chem. 16 (2009) 4536.
[9] R.K. Katiyar, R. Singhal, K. Asmar, R. Valentin, R.S. Katiyar, J. Power Sources 194 (2009) 526.
[10] H.J. Yue, X.K. Huang, D.P. Lv, Y. Yang, Electrochim. Acta 54 (2009) 5363.
[11] H. Li, Z. Wang, L. Chen, X. Huang, Adv. Mater. 21 (2009) 1.
[12] Z. Yang, D. Choi, S. Kerisit, K.M. Rosso, D. Wang, J. Zhang, G. Graff, J. Liu, J. Power Sources 192 (2009) 588.
[13] O. Mao, R.A. Dunlap, J.R. Dahn, J. Electrochem. Soc. 146 (1999) 405.
[14] S.-H. Ng, J. Wang, D. Wexler, K. Konstantinov, Z.-P. Guo, H.-K. Liu, Angew. Chem. Int. Ed. 45 (2006) 6896.
[15] K.D. Kepler, J.T. Vaughey, M.M. Thackeray, Electrochem. Solid State Lett. 2 (1999) 307.
[16] A.S. Aricò, P. Bruce, B. Scrosati, J.-M. Tarascon, W. Van Schalkwijk, Nat. Mater. 4 (2005) 366.
[17] P.L. Taberna, S. Mitra, P. Poizot, P. Simon, J.-M. Tarascon, Nat. Mater. 5 (2006) 567.
[18] Y. Yu, C.-H. Chen, J.-L. Shui, S. Xie, Angew. Chem. Int. Ed. 44 (2005) 7085.
[19] E. Hosono, S. Fujihara, I. Honma, M. Ichihara, H. Zhou, J. Electrochem. Soc. 153 (2006) A1273.
[20] M. Winter, R.J. Brodd, Chem. Rev. 104 (2003) 4245.
[21] M.-Y. Cheng, C.J. Pan, B.-J. Hwang, J. Mater. Chem. 19 (2009) 5193.
[22] S. Zhu, H. Zhou, M. Hibino, I. Honma, M. Ichihara, Adv. Funct. Mater. 15 (2005) 381.
[23] D.R. Rolison, Science 299 (2003) 1698.
[24] P. Poizot, S. Laruelle, S. Grugeon, L. Dupont, J.-M. Tarascon, Nature 407 (2000) 496.
[25] S.A. Needham, G.X. Wang, H.K. Liu, J. Power Sources 159 (2006) 254.
[26] S. Jun, S.H. Joo, R. Ryoo, M. Kruk, M. Jaroniec, Z. Liu, T. Ohsuna, O. Terasaki, J. Am. Chem. Soc. 122 (2000) 10712.
[27] H. Zhou, S. Zhu, M. Hibino, I. Honma, M. Ichihara, Adv. Mater. 15 (2003) 2107.
[28] M. Dollé, P. Poizot, L. Dupont, J.-M. Tarascon, Electrochem. Solid-State Lett. 5 (2002) A18.
[29] S. Grugeon, S. Laruelle, L. Dupont, J.-M. Tarascon, Solid State Sci. 5 (2003) 895.